http://dx.doi.org/10.5935/0103-5053.20140296

J. Braz. Chem. Soc., Vol. 26, No. 3, 434-450, 2015.
Printed in Brazil - ©2015 Sociedade Brasileira de Química
0103 - 5053 $6.00+0.00

Article

Experimental and Theoretical Studies of Volatile Corrosion Inhibitors Adsorption on Zinc Electrode

Deiver A. Teixeira,[a,b] Marco A. G. Valente Jr.,[a] Assis V. Benedetti,*[,a] Gustavo T. Feliciano,[a] Sebastião C. da Silva[c] and Cecílio S. Fugivara[a]

[a]*Instituto de Química de Araraquara, Universidade Estadual Paulista "Júlio de Mesquita Filho" (UNESP), R. Prof. Francisco Degni, 55, P.O. Box 355, 14800-900 Araraquara-SP, Brazil*

[b]*Instituto Federal do Mato Grosso (IFMT), Campus Cuiabá - Bela Vista, Av. Juliano Costa Marques, s/n, 78050-560 Cuiabá-MT, Brazil*

[c]*Instituto de Química, Universidade Federal do Mato Grosso (UFMT), Av. Fernando Corrêa da Costa, 2367, 78060-900 Cuiabá-MT, Brazil*

This study evaluates the interaction of volatile corrosion inhibitors (VCIs) of the amino group with the zinc or zinc oxide surface by means of computational calculations using density functional theory (DFT) and comparing with experimental methods such as electrochemical impedance spectroscopy (EIS) and wet chamber tests. The application of these methods allowed indicating the most promising VCI and understanding its mechanism of action. Thus, after the vaporization of VCI molecules, they condense on the surface and form a protective film or a film with oxidizing characteristic, thereby preventing the corrosive action of the chemical species present in the environment.

Keywords: volatile corrosion inhibitors, density functional theory, electrochemical impedance spectroscopy, wet test chamber

Introduction

Organic molecules containing the amino functional group could be efficient corrosion inhibitors on zinc surface.[1,2] To work as inhibitors, these compounds must have some characteristics in their chemical structure, such as high electron density, contain elements like oxygen, sulfur, nitrogen or π bonds.[3,4] Humidity, temperature variations and atmospheric pollutants can lead to partial or total deterioration of a given metallic material.[2] This is why, after fabrication of any metallic part, its surface needs some chemical treatment, in order to avoid deterioration during transport and storage. The most employed method to protect metallic parts from corrosion is to use volatile corrosion inhibitors (VCIs), which are generally used to impregnate plastic films, enveloping the metallic parts.[4]

The VCI compounds must have adequate vapor pressure to fill the environment, keeping its efficiency against corrosion by the necessary time, with the parts completely covered by the inhibitor, independent of its shape.[2,5,6] The inhibitor molecule vaporizes and is adsorbed at the metallic surface in the gaseous state, in the neutral non-protonated form.[6] In this way, after the VCI vaporization process and its adsorption to the metal, corrosion inhibition can happen by means of the formation of a protecting film and also the saturation of the air with the VCI vapor.[7] The length of time of adsorption depends on the kinetic energy and the number of molecules on the surface, surface roughness and temperature variation. Metal surfaces can be thought as a bidimensional plane full of potential energy wells, where the VCI and other compounds from the surroundings compete for the minimum energy sites.[8]

In the literature, several studies can be found about the efficiency of different VCIs, using measurements in wet test chamber, electrochemical assays and theoretical computational modeling.[9] Wet chamber assays better reproduce the environment conditions of humidity and temperature cycling, but demand a long period of tests.[10] In order to reduce the amount of time with respect to the wet chamber assay, electrochemical assays, specially by means of electrochemical impedance spectroscopy (EIS) and electrochemical noise analysis (ENA) can be done.[11]

*e-mail: benedeti@iq.unesp.br

In order to corroborate the results and to provide a better understanding of the process, computational calculations can also be employed to analyze the metal-inhibitor interaction.[12-14] These calculations can be performed in different conditions (dry, solvent, etc.), and usually give information about the system geometry, molecular orbitals, electronegativity, interaction energy, electron density and electrostatic potential, among others. In this sense, several authors have correlated the frontier molecular orbitals, highest occupied molecular orbital (HOMO) and lowest unoccupied molecular orbital (LUMO) and energy difference (ΔE) between E_{LUMO} and E_{HOMO}, atomic charges and dipole moment with inhibition efficiency obtained in experimental methods.[14]

In the last years, there was a significant increase in computers' computational power, and also the development of accurate electronic structure calculation methodologies demanding less computational power, such as density functional theory (DFT) allowed the treatment of systems composed of several atoms. However, the computational effort still increases as the cube of the number of electrons in the system, and thus, insertion of metals in the system greatly increases the computational effort, sometimes invalidating the simulation. To overcome this difficulty while retaining quality in the results, the "our own n-layered integrated molecular orbital and molecular mechanics" (ONIOM) methodology is usually employed,[15] where the system is partitioned in "layers", where each layer is treated by a different level of calculation. This reduces the computational effort in areas where a simpler description already captures the essence of the studied phenomenon. In each layer, the chosen treatment could be classical, semiempirical, or even quantum mechanical, with different basis sets.[16]

DFT has become a very popular tool for computer simulation, due to its lower computational cost when compared to Hartree-Fock,[17] or other complex wave function-based methods. In this type of calculation, it is necessary to use mathematical functions, for example, Gaussian functions, which form the basis set. Usually, the basis set is atom-centered, and the linear combination of these functions give rise to the molecular orbitals (the LCAO approach). In this approach, all valence electrons have influence on the stability of the molecule. When the atomic orbitals are combined, they form molecular orbitals, and this gives rise to a new set of energetic states which corresponds to new distributions of the electronic density.[15]

The electronic interaction can be extrapolated for interactions between compounds in different physical states, as the case of the metal inhibitor interaction.[8] This adsorption process can be divided in: (*i*) physical interactions, also called physisorption, which do not involve formation of new covalent bonds between the surface and the adsorbate. The dominant forces in this process are electrostatic and Van der Waals forces; (*ii*) chemical interactions, also denoted chemisorption, which produce changes in the electronic structure by a chemical reaction, forming new covalent bonds.[11]

Due to the great relevance of the VCIs in the metallurgical industry and the demand for more efficient inhibitors for different materials and different environmental conditions, one of the objectives of this work is to correlate the theoretical data about some commonly used amine-based VCIs with the experimental results, in order to design new VCIs. Therefore, the interaction between the zinc surface with the VCIs cyclohexylamine (CHA), dicyclohexylamine (DCHA), ethanolamine (ETA) was studied by EIS using zinc electrodes to obtain the kinetic parameters of the electrochemical process in the presence of the VCI. Furthermore, zinc was submitted to wet chamber assays, and optical microscopic images were subsequently taken. Previous work[1] with CHA and DCHA displayed inhibition efficiency higher than 70% for corrosion of zinc, iron and copper. As for ETA, passivation was observed when the assay was made on steel.[2] In the available literature, no theoretical calculation relating the interaction of the previously cited VCIs and zinc/zinc oxide surfaces was found.

The ONIOM method (B3LYP/6-31G:PM6) was employed for the study of the interaction between zinc and zinc oxide surfaces and the VCIs, and the results were related to the experimental measurements. In the geometry optimization calculations, DFT (B3LYP/6-31G)[18,19] calculations were performed.

Methodology

In the present study about VCI-zinc/zinc oxide surface interaction, the theoretical calculations were correlated with results obtained from open circuit potential measurements (E_{OC}), EIS, scanning electron microscopy with a field emission gun (SEM-FEG) and optical micrograph (OM). With respect to the theoretical results, the corresponding frontier molecular orbitals, Mulliken charges and interaction energies were considered.

The chemical structure, names and abbreviations for the studied VCIs are described in Table 1.

In aqueous solution, these compounds can react with water, generating the hydroxyl group OH^- as illustrated by the equations 1-3, and consequently, the pH of the solution shall rise.[20] Figure 1 shows the relation between the pH with the percentage of each species, obtained by the MarvinSketch[18] program. In this way, it is possible to

Table 1. Chemical structure, name and abbreviation of the VCI compounds

Chemical structure	Name	Abbreviation
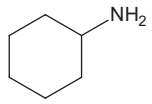	Cyclohexylamine	CHA
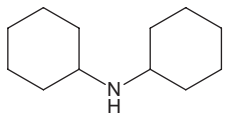	Dicyclohexylamine	DCHA
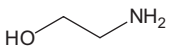	Ethanolamine	ETA

observe that amines increase the alkalinity of the solution to pH ≥ 11.

$$ETA + H_2O \leftrightarrow ETAH^+ + OH^- \quad \text{Miscible} = 20\ °C \quad (1)$$

$$CHA + H_2O \leftrightarrow CHAH^+ + OH^- \quad \text{Miscible} = 20\ °C \quad (2)$$

$$DCHA + H_2O \leftrightarrow DCHAH^+ + OH^- \quad \text{Solubility} = 5 \times 10^{-3}\ \text{mol L}^{-1}\ \text{at } 20\ °C \quad (3)$$

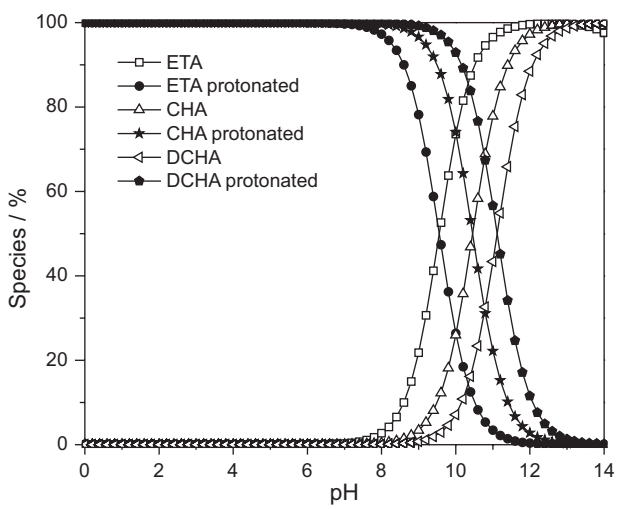

Figure 1. Percentage of the observed species *vs.* the pH of aqueous solutions diagrams of ETA, CHA and DCHA amines. Diagrams obtained by the MarvinSketch[18] program.

For example, from Figure 1, at pH 11 DCHA, CHA and ETA display the non-protonated species percentages of 60, 70 and 95, respectively. In molecule adsorption studies over the zinc surface, zinc oxide should also be considered, whose formation is thermodynamically favored in the presence of water or oxygen.[21] In other works[22,23] at least three types of zinc oxide surfaces are considered, and from these, the lowest-energy one is the mixed-terminated (1 0 1 0)-surface. Therefore, calculations for VCI adsorption on zinc oxide surface were also performed, due to the possible presence of zinc oxide on zinc surface, during the electrochemical measurements.[21]

Theoretical section

Quantum chemical calculations were performed at the DFT level, due to the lower computational cost when compared to *ab initio* Hartree-Fock and sufficient accuracy, observed in several other works.[24-28] The GAUSSIAN 09W[25] package was used for all calculations, and the B3LYP[26] exchange correlation functional was employed, along with a 6-31G basis set,[27] and GaussView[28] package to build the figures.

The ONIOM method (B3LYP/6-31G:PM6) was used to calculate the interaction energy of each VCI with a model zinc surface (6 Å × 7 Å × 2 Å unit cell, optimized with 157 atoms) and a model zinc oxide surface (5 Å × 5 Å × 2 Å unit cell, optimized with 207 atoms). All calculations took into account the water, using the IEFPCM[29] formalism, in GAUSSIAN 09W program.

The VCI-surface interaction energies were studied in two different setups: first, a potential energy surface was obtained by approximating one VCI molecule to the surface, and within each distance, the coordinates are optimized with respect to the energy. The coordinate used to describe the VCI-surface separation is the VCI nitrogen atom and the closest zinc atom. In this case, the interaction energy, $E_{int(scan\ VCI)}$, was obtained from the total energy of the system, E_{total}, minus the individual energies of the VCI, E_{VCI}, and the metal surface, $E_{surface}$, as described by the following equation:[27,28]

$$E_{int(scan\ VCI)} = E_{total} - E_{VCI} - E_{surface} \quad (4)$$

In the second approach, the interaction energy among the VCI molecules was considered (a "lateral" interaction energy), over the metal surface. In this case, the total interaction energy of the system, $E_{int\ total}$, is a sum of the interaction energy of the VCI molecules and the surface (a "vertical" interaction), $E_{int(VCI/Zn\ surface)}$, and the interaction energy between the VCI molecules only (the lateral interaction), $E_{int(VCI\ molecules)}$. The total interaction energy for the addition of each VCI molecule can be calculated as:[30,31]

$$E_{inttotal} = E_{int\left(\frac{VCI}{Zn}surface\right)} - E_{int(VCI\ molecules)} \quad (5)$$

In order to clarify the pictures shown in this work, spheres of different sizes, symbols and colors were attributed for each chemical element, as shown in Figure 2.

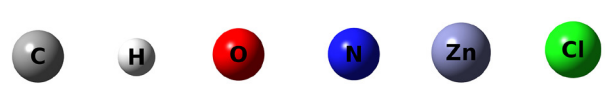

Figure 2. Representation of each element in the VCI and surface molecular structures.

Experimental section

The CHA, DCHA and ETA compounds (Sigma Aldrich, AR grade) were used as received. Electrochemical measurements on zinc electrode were performed in the following solutions: (*i*) 0.1 mol L^{-1} NaCl (pH 11 adjusted with NaOH) with and without amines (CHA, DCHA and ETA) in the 5×10^{-3} mol L^{-1} concentration. The choice of the amine concentration was limited by the solubility of DCHA.[32] Despite this fact, it is experimentally observed that DCHA displays a lower solubility than what is actually referenced.[32,33]

Zinc plates (99.9%) with 2 cm × 2 cm were polished with sandpapers of 600 and 1200 granulometry and polishing cloth with alumina suspension (particle size of 0.3 µm), and sonicated in isopropanol for 5 min.[34] The geometric area of the working electrode exposed to the solution was 1 cm^2. The electrochemical assays were made right after, in a Pyrex® glass cell, with a spiral shaped platinum wire as auxiliary electrode, and $Ag/AgCl/KCl_{sat}$ as reference electrode. All electrode potentials were referenced to the $Ag/AgCl/KCl_{sat}$ electrode. The open circuit potential (E_{OC}) was recorded for 10 h for the assays with and without the amines. After the stabilization of the open circuit potential, EIS measurements were made by applying a sinusoidal signal of 10 mV (rms) on the E_{OC}, in frequencies ranging from 10 mHz to 10 kHz, and recording 10 points *per* decade. The electrochemical measurements were recorded in an EG&G PAR 283 and FRA Solartron 1255 potentiostat, controlled by the PAR M398 program. The EIS data were treated with the BOUKAMP[35] program. Impedance diagrams for the zinc electrode were obtained in a 0.1 mol L^{-1} NaCl aqueous solution (pH 11, adjusted with 0.1 mol L^{-1} NaOH) with and without the addition of 5×10^{-3} mol L^{-1} of ETA, CHA and DCHA. The DCHA solution is being regarded, in this work, as a saturated solution, for the expressed value of 5×10^{-3} mol L^{-1} corresponds to DCHA solubility.

Wet chamber assays were performed as established by the IEC 6008-2-30 Standard Practice of the International Electrotechnical Commission.[10] Zinc plates were kept in the wet chamber in the presence and absence of the VCIs for 7 days, under humidity and temperature cyclic conditions as established by the IEC 6008-2-30 Standard Practice. The thermal cycle defined for 1 day is initiated at 25 ºC for 6 h and relative humidity (RH) of 98%, submitted to heating until it reaches 55 ºC after 3 h. The system is kept at this temperature for 9 h and RH 95%. After this, the temperature is diminished to 25 ºC after 3 h and the system is kept for more 3 h at 25 ºC, ending the cycle. After 7 cycles, the samples were naked eye analyzed and optical micrograph images were taken using an optical stereomicroscope QUIMIS with 80× magnification. The surfaces of zinc plates before and after the immersion in 0.1 mol L^{-1} NaCl solution in the presence and absence of VCIs for 15 days were analyzed by scanning electron microscope using a Jeol JSM 7500F SEM-FEG coupled with a Thermo Noran System six energy dispersive X-ray spectrometer (EDS).

Results and Discussion

Molecular orbital analysis

Figures 3-5 show the lowest energy configuration of the VCIs and the distribution of the frontier molecular orbitals HOMO and LUMO, obtained by the quantum chemical calculations at the B3LYP/6-31G level, in aqueous environment. The interaction of these orbitals with the zinc/zinc oxide surfaces was also analyzed.

The CHA, DCHA and ETA VCIs possess the nitrogen atom in the functional amino group, already characterized by other studies[1,31,36] as an electron donor group, consequently inhibition corrosion by donating electrons to the metal of interest. This way, it is observed that, in CHA, DCHA and ETA, the HOMO (Figures 3b, 4b and 5b) is mainly located on the nitrogen, and the LUMO is spread all over the molecule (Figures 3c, 4c and 5c). Both frontier orbitals are of interest, by the donor characteristics of HOMO and the acceptor characteristics of LUMO it is possible to make reference to the corrosion inhibition process.[31,37]

Figure 6 shows the frontier orbital energies of the VCI with respect to Figures 4 and 5. The difference between the energies of the frontier orbitals, also denominated as HOMO-LUMO gap, as well as the individual values of each orbital can be compared to the corrosion inhibition efficiency.[38] HOMO orbitals with higher energy donate electrons more easily to the *d* orbitals of the metals. On the other hand, LUMO orbitals with lower energy have more tendency to receive electrons from the *d* orbital of metals.[27] Figure 6 shows the following order in HOMO energy for the VCIs: ETA > CHA > DCHA, while for the LUMO energy, the order is: CHA > ETA > DCHA. The HOMO-LUMO gap of molecules in the ground state refers to the molecule corrosion inhibition activity, that is, the smaller the gap, the higher the molecule activity.[38] The value of the gaps follows the order: DCHA << ETA < CHA.

The molecular orbitals of the VCIs give important information with respect to the active site and reactivity of the VCI, and this parameter is generally related to the corrosion inhibition efficiency of the VCIs.[13] However, these informations can be better accessed considering the

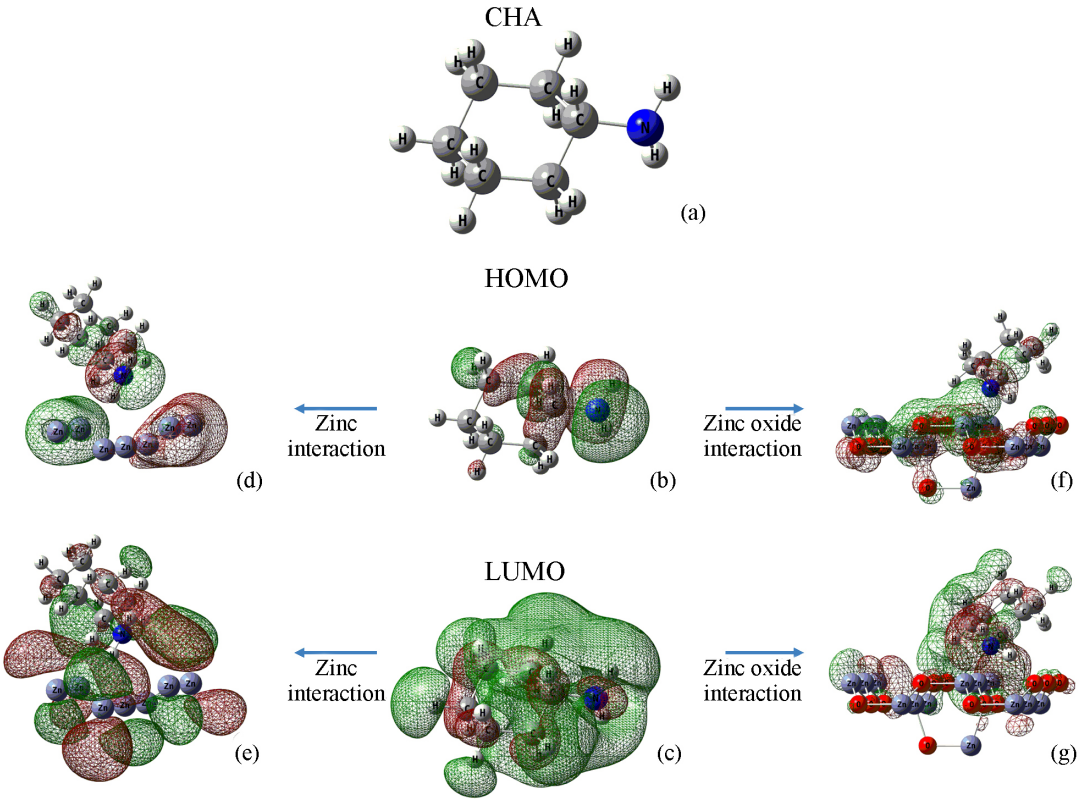

Figure 3. Spatial distribution of the frontier molecular orbitals of CHA: (a) chemical structure; (b) HOMO orbital; (c) LUMO orbital; (d) HOMO/zinc surface interaction; (e) LUMO/zinc surface interaction; (f) HOMO/zinc oxide surface interaction; and (g) LUMO/zinc oxide surface interaction.

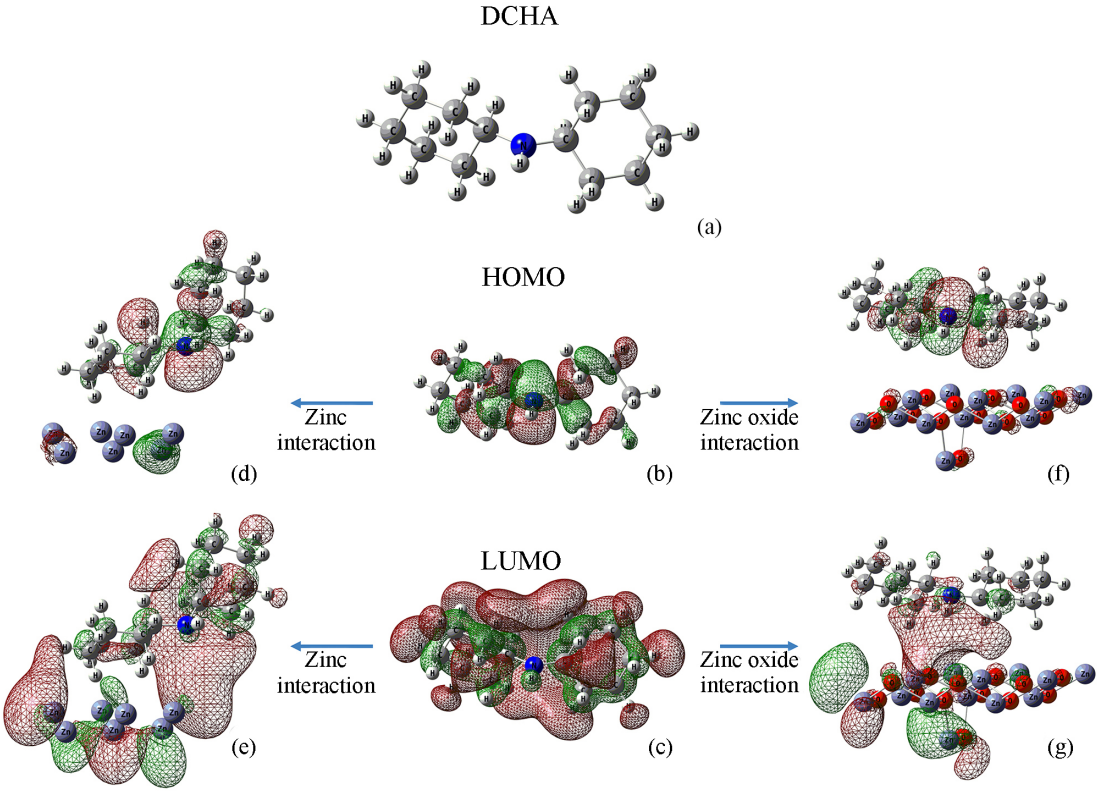

Figure 4. Spatial distribution of the frontier molecular orbitals of DCHA: (a) chemical structure; (b) HOMO orbital; (c) LUMO orbital; (d) HOMO/zinc surface interaction; (e) LUMO/zinc surface interaction; (f) HOMO/zinc oxide surface interaction; and (g) LUMO/zinc oxide surface interaction.

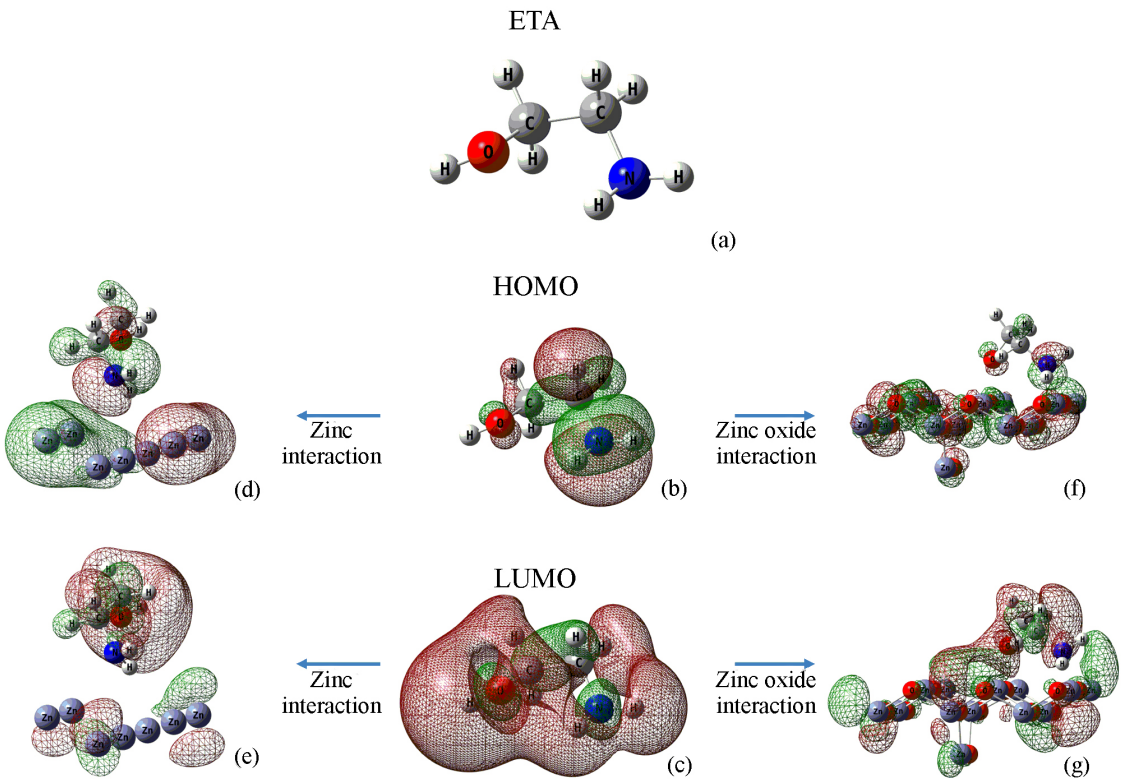

Figure 5. Spatial distribution of the frontier molecular orbitals of ETA: (a) chemical structure; (b) HOMO orbital; (c) LUMO orbital; (d) HOMO/zinc surface interaction; (e) LUMO/zinc surface interaction; (f) HOMO/zinc oxide surface interaction; and (g) LUMO/zinc oxide surface interaction.

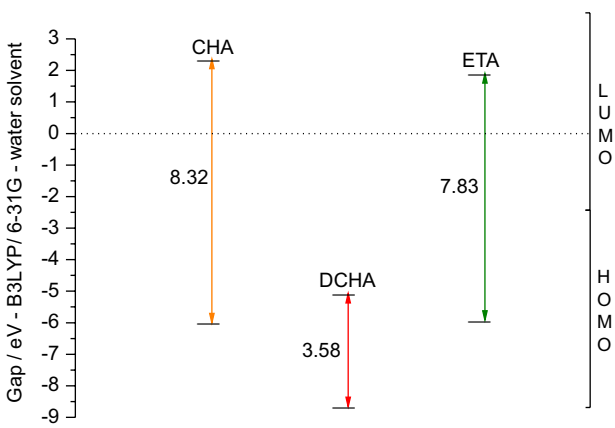

Figure 6. VCI energy gaps.

frontier orbitals, which determine the way the molecule interacts with other species, with the electronegativity and chemical hardness of the metal.

For this purpose, Koopmans[39] theorem can be used, and the electronegativity and electron affinity can be determined from the frontier orbitals. In this case, the HOMO energy is related to the ionization potential (IP), which measures the availability of a molecule for sharing or donating its electrons. The LUMO energy is related to the electron affinity (EA) of the molecule, i.e., its ability to attract electrons:

$$IP = -E_{HOMO} \quad (6)$$

$$EA = -E_{LUMO} \quad (7)$$

Electronegativity (χ) and chemical hardness (η)

$$\chi = \frac{IP + EA}{2} \quad (8)$$

$$\eta = \frac{IP - EA}{2} \quad (9)$$

for zinc, reference values are found in literature:[40] IP_{Zn} = 9.39 eV and AE = –0.49 eV, eletronegativity, χ_{Zn} = 4.45 eV, and global hardness, η_{Zn} = 4.94 eV. Using equations 6-9, the IP, EA, χ and η values are obtained for all VCIs (Table 2). In this table, the fraction of transferred electrons (ΔN)[41] from the inhibitor to zinc can also be found, as depicted in equation 10.

$$\Delta N = \frac{\chi_{metal} - \chi_{inhibitor}}{2\,(\eta_{metal} + \eta_{inhibitor})} \quad (10)$$

where χ_{metal} and $\chi_{inhibitor}$ indicate the eletronegativity, η_{metal} and $\eta_{inhibitor}$ the global hardness, both respectively to the metal and inhibitor.

Table 2. Quantum chemical parameters calculated for the VCIs interacting with zinc

Inhibitor	E_{HOMO} / eV	E_{LUMO} / eV	*IP* / eV	*EA* / eV	$\chi_{inhibitor}$ / eV	$\eta_{inhibitor}$ / eV	ΔN_{Zn}
CHA	–5.94	2.39	5.94	–2.39	1.77	4.16	0.15
DCHA	–8.60	–5.02	8.60	5.02	6.81	1.79	–0.18
ETA	–5.87	1.95	5.87	–1.95	1.96	3.91	0.14

According to the studies of Lukovits,[21] if $\Delta N < 3.6$ the inhibition of the corrosion happens by transference of electrons from the inhibitor to the metal. In case the value is greater than 3.6 the transference occurs from the metal to the inhibitor. In Table 2, for all inhibitors, the values of ΔN are smaller than the reference value, and in this sense, there is electron transfer from the VCIs to the metal. As for the absolute value, there are significant variations between DCHA and CHA/ETA.

VCI interaction with zinc and zinc oxide surface

Using the ONIOM method[42] the interaction of the VCIs with the zinc/zinc oxide surfaces was analyzed. In these calculations, 7 zinc atoms from the zinc surface and 26 atoms of zinc and oxygen from the zinc oxide surface, in an hexagonal arrangement with a central Zn/ZnO group at a lower height with respect to the hexagonal region, in the surface, along with the VCI molecule were treated quantum mechanically (B3LYP/6-31g). The other zinc/oxygen atoms were treated at the semiempirical level, PM6. Figures 7 and 8 show spheres with different dimensions: the greater ones were treated by DFT, while the smaller ones were treated semiempirically. The initial configurations were obtained by optimization with the nitrogen group of the VCI initially at a distance of 4 Å from the zinc surface, with the nitrogen in the atop configuration, with respect to the central zinc atom. Only this adsorption site was considered, to the heavy computational cost of DFT B3LYP calculations, compared to other simpler functionals. Besides, the considered VCIs are somewhat rigid (specially in the case of CHA and DCHA) and bulky, compared to the adsorption site, and due to those reasons, other interactions cited were not explored at the moment. However, in order to keep consistency in the comparison of the metal-molecule interaction, all calculations of the 3 VCIs and the two surfaces were made at the same adsorption site and the same atomic arrangement in the surface, with the same initial distance of the nitrogen group from the central atom of the surface.

Figure 7 shows that the nitrogen atom has great importance in the interaction with the zinc surface, in the CHA and ETA compounds, while in DCHA, nitrogen does not get close to the surface, due to the steric hindrance caused by the cycloalkanes. In Figure 8, the amino group of the CHA, DCHA and ETA are next to the surface of the oxide, and the hydroxyl group of the ETA also interacts, and this shows the strongest interaction when compared to CHA (Figure 5f and g). The proximity of these surface groups indicates that they are responsible for the protective or destructive action over the zinc oxide surface.

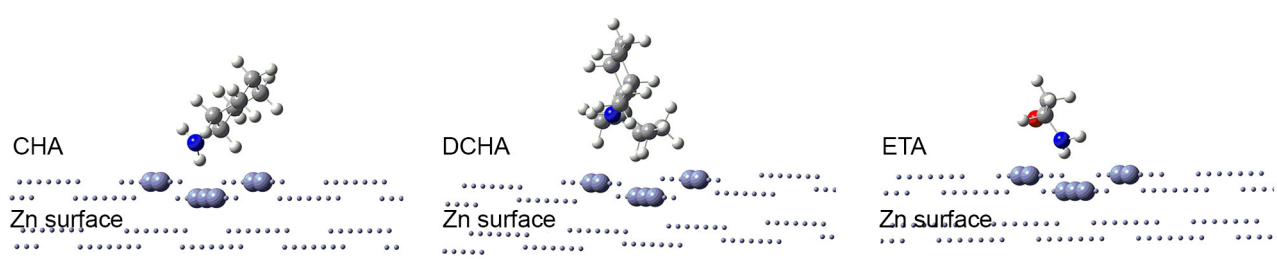

Figure 7. Minimum energy configuration in the VCI-zinc surface interaction.

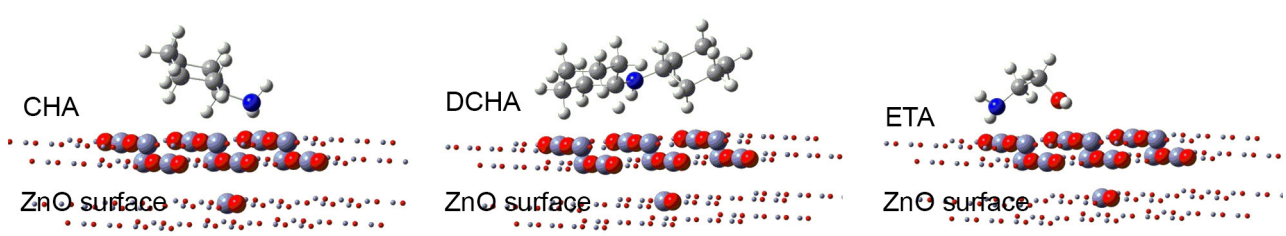

Figure 8. Minimum energy configuration in the VCI-zinc oxide surface interaction.

Despite the highlighted information regarding the spatial dispositions of the VCI molecules on the surfaces, the analysis of the frontier orbitals is also important. These orbitals were calculated for the system in a local minimum energy configuration, regarding only the quantum mechanical region. Interactions of these orbitals with the zinc/zinc oxide surfaces are depicted in Figures 3d-g, 4d-g and 5d-g. The CHA, DCHA and ETA compounds have their frontier orbitals partially shifted towards the zinc/zinc oxide surface (Figures 3d-g, 4d-g and 5d-g), except for DCHA (Figure 5f) whose HOMO interaction only happens with the oxygen atoms.

Potential energy scan and Mulliken charge analysis

The energy of the metal-VCI system was calculated as the distance between the metal and the VCI molecule is increased. For this purpose, starting from the optimized system (VCI/zinc surface or VCI/zinc oxide surface), denoted as "starting point" (Figures 7 and 8), the molecule is moved to a distance of 6 Å from the surface, and then the potential energy surface (PES) is obtained.[43] For the minimum energy interaction and sequentially after each increment of 1 Å in the separation, the sum of Mulliken charges of the surface atoms and the sum of the charges of the VCI atoms were calculated. In this way, the system is evaluated by the interaction energy between VCI and the zinc surface, the global energy difference, and also, the respective Mulliken charges in each configuration (Figure 9). The PES in Figure 9a-c shows the interaction energy for the departure from the minimum energy configuration of the VCI with respect to the zinc surface. Thus, among the compounds containing the amine group, DCHA (Figure 9b) presents greater interaction energy in the minimum energy configuration (Table 3). For CHA (Figure 9a) and ETA (Figure 9c) the interaction energies in the "starting point" are very close, and the interaction energy difference between the starting point and the final point is 13.1 kcal mol^{-1} for CHA and 8.6 kcal mol^{-1} for ETA. Therefore, the energy drop in 6 Å is more pronounced for CHA, DCHA and ETA at the zinc surface.

Following the same theoretical procedure, Figure 9d-f shows the interaction energies of the VCI with the zinc oxide surface. In this case, the energetic behavior of the system is similar to the VCI/zinc surface system. In the local minimum energy configuration DCHA (Figure 9e) is the compound with the strongest interaction energy, followed by ETA. The interaction energy difference between the starting point and the final point for DCHA is 6.2 kcal mol^{-1}, and 52.6 kcal mol^{-1} for ETA (Figure 9c), which can be attributed to the interaction between the ETA alcoholic oxygen and the zinc oxide surface. Finally, CHA (Figure 9a) shows the interaction energy of –22.7 kcal mol^{-1} with a total difference between starting and ending point of 26.8 kcal mol^{-1} (Table 3).

The significant value of DCHA/zinc oxide surface interaction energy is similar to the DCHA/zinc surface interaction energy. Population analysis[44] allowed obtaining of the Mulliken charges. Figure 9 shows the summation of the charges in the VCI molecules and the zinc surface. Negative charge means a higher electron density (reductive state, attributed to a certain group of atoms). On the other hand, positive charge means a lower electron density, which could be compared to an oxidative state.

For the interaction with zinc oxide surface, the order observed for charge density on the surface was: CHA > DCHA > ETA. Since the charges add to zero, the previous sequence refers to the positive charge of the VCIs. Despite the limitations for the derivation of Mulliken charges,[45] the calculated values are consonant with the interaction energy between the VCIs and the surface. It can be noted that there is charge transfer from the molecule to the surface.

VCI adsorption over zinc surface - film formation

In order to understand the interactions that occur among the VCI molecules (lateral interactions) the zinc surface area was increased and more than one VCI molecule was added. In this sense, the VCI molecules were added one by one, and after each addition, the geometry was optimized again and the interaction energy calculated, which includes the interaction of VCI molecules with the zinc surface and the lateral interaction between the VCI molecules (equation 6). This is, by no means, a definite structure of the film, as other factors must be taken into account at the moment the film is formed, such as the vapor pressure and temperature, but still, it gives a nice idea of the lateral interaction strength, when maximum surface coverage is attained.

In these calculations, the ONIOM method was applied, but differently from the previous topic, the metallic surface is treated at the classical level (molecular mechanics, MM),[46] and the VCI molecules were treated at the quantum level, using DFT/B3LYP 6-31G. In these calculations, the vertical interaction energy does not take into account electronic charge transfer effects between the VCIs and the metal surface, which limits the conclusions regarding this type of interaction. However, the lateral interaction energy among VCI molecules can be evaluated.

Figure 10 depicts the adsorption of 12 molecules of each VCI, separately, over the zinc surface. In a general way, the molecules adhere to the surface in a relatively organized way. For CHA (Figure 10a, b), DCHA (Figure 10c, d) and ETA (Figure 10e, f) the structures suggest in a reproductive

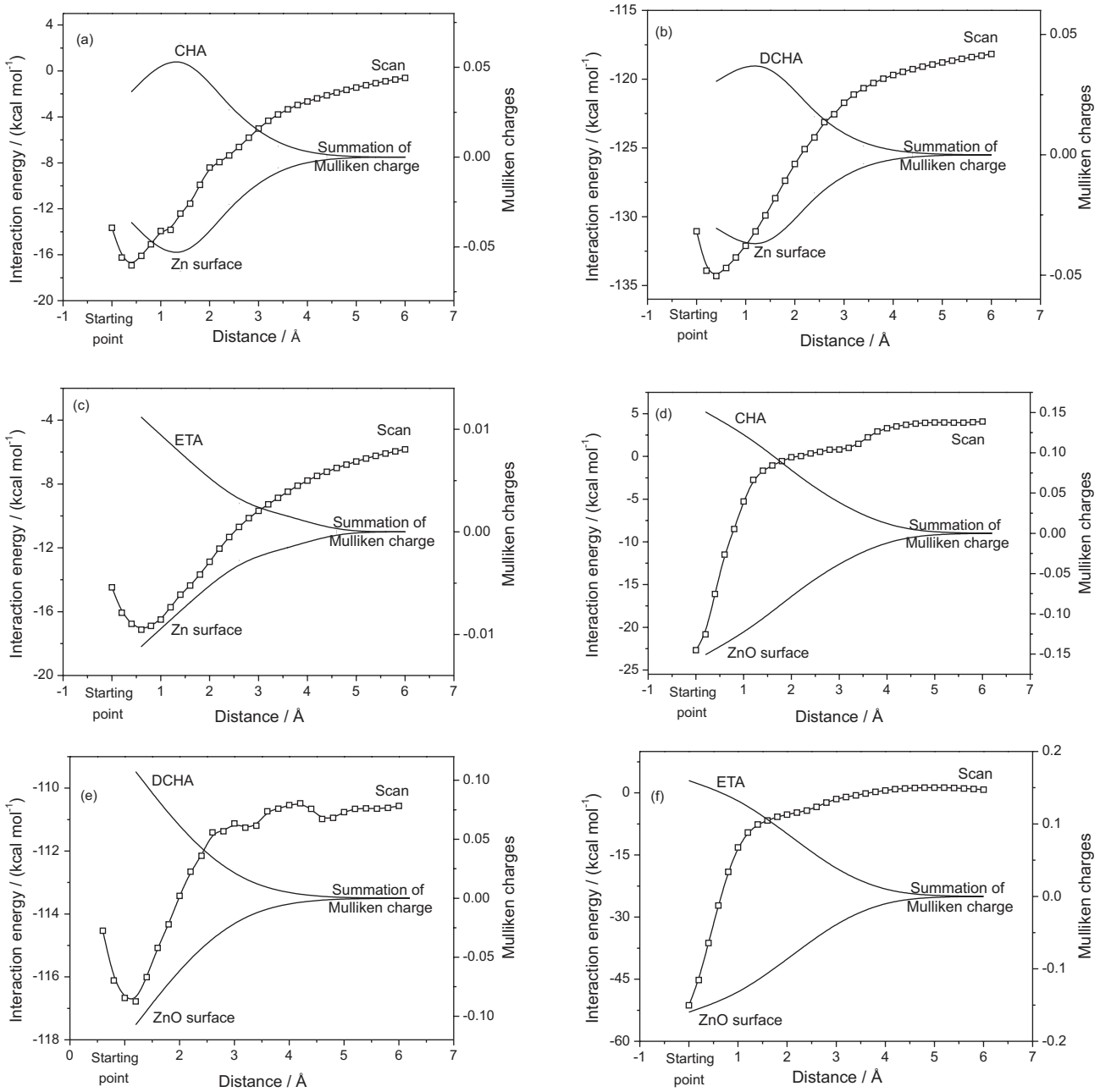

Figure 9. Potential energy surfaces (in terms of the interaction energy) and Mulliken charges summation for the VCIs on the zinc surface [(a) CHA, (b) DCHA and (c) ETA] and zinc oxide [(d) CHA, (e) DCHA and (f) ETA].

Table 3. Interaction energies at the minimum energy configuration

System	Interaction energy, minimum energy configuration / (kcal mol^{-1})	Energy difference, minimum energy configuration at 6Å distance
Zn surface + CHA	–17	13.1
Zn surface + DCHA	–134.3	12.9
Zn surface + ETA	–17	8.6
ZnO surface + CHA	–22.7	26.8
ZnO surface + DCHA	–116.7	6.2
ZnO surface + ETA	–51.3	52.6

six-membered ring shape, with one molecule in the center for CHA and ETA, and five-membered and six-membered rings for DCHA. In the lateral interaction of CHA and DCHA, it can be noted that the nitrogen has the lone electron pair pointing towards the surface. However, in ETA, nitrogen is pointing to the hydroxyl group, favoring the lateral interaction.

Figure 11 shows that as more VCI molecules are added to the system, the lateral interactions with the zinc surface show different behavior for each compound. The total interaction energies are more pronounced for DCHA (Figure 11b), but this energy is practically entirely in

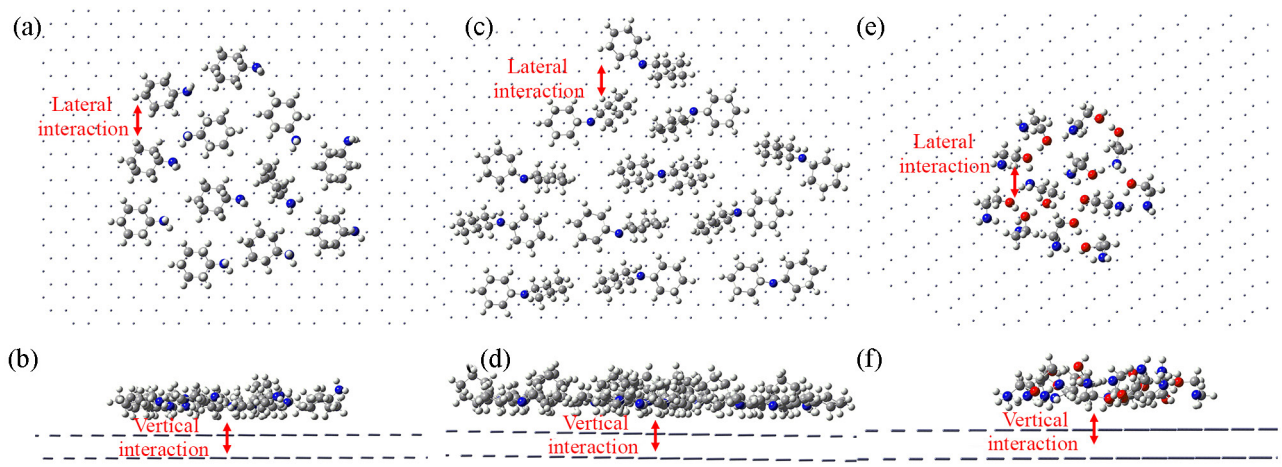

Figure 10. Formation of the VCI film over the zinc surface, horizontal and vertical view. (a) and (b) 12 CHA; (c) and (d) 12 DCHA; and (e) and (f) 12 ETA.

the lateral interaction between the molecules, being the vertical interaction less than 10% of the total energy. Even so, this value is still greater than the vertical interaction energy of CHA (Figure 11a) and ETA (Figure 11c), that is, the vertical interaction energy for the 12 molecules of DCHA is around –120 kcal mol^{-1}, –60 kcal mol^{-1} for CHA and –40 kcal mol^{-1} for ETA. Both ETA and DCHA possess the greatest part of the total interaction energy in the lateral interaction, and this can be attributed to hydrogen bonding in ETA and the chemical similarity for DCHA. On the contrary, CHA (Figure 11a) possesses most of the total energy in the vertical interaction. The lateral interaction occurs, but stabilizes around –10 kcal mol^{-1}.

Figure 12 shows the average of the energy for the lateral interaction. Among the CHA, DCHA and ETA compounds, it can be seen that DCHA has an expressive lateral interaction, being subtly intensified as more molecules were are added. This behavior could be attributed to the non-polar character of cycloalkanes, which present low solubility in aqueous solvent.[32,33] As for ETA, the addition of molecules at the surface increases the lateral interaction until 7 molecules are added. From this point on, addition of more molecules no longer alters the average energy. This could suggest a six-membered ring format, with a molecule at the center (Figure 10e). CHA has a low lateral interaction, on average, and the addition of other molecules does not intensify this kind of interaction.

In regular environments, zinc suffers the influence of many other agents, like temperature, humidity, oxidizing species, among others. The theoretical calculation performed in this work considered an ideal situation where VCI interacts with the surface in the presence of water as an implicit solvent. Despite the simplicity of the approach, there is a good agreement with the experimental data, which will be described and discussed in the following sections.

Open circuit potential

Figure 13 shows the variation of the open circuit potential (E_{OC}) of the zinc electrode in 0.1 mol L^{-1} NaCl (pH 6.5 and 11) solution in the presence and absence of CHA, DCHA and ETA.

As for the NaCl solution (pH 6.5, Figure 13, curve a) the potential continuously decreases since the beginning of the measurement (–1.03 V), and even after 10 h (–1.07 V) it keeps decreasing. In 0.1 mol L^{-1} NaCl solution (pH 11, curve b), the initial potential is –0.96 V, decreases continuously until it reaches the value of –1.05 V after 10 h without reaching stabilization. In the NaCl solutions containing amines (pH ca. 11, curves c-e), it is stabilized at different immersion times, depending on the amine: DCHA (–0.99 V after around 3 h); CHA (–0.99 V after ca. 6 h) and ETA (–1.02 V after ca. 8 h). The lowest potential was observed for the solution containing chloride, at pH 6.5, suggesting that the zinc oxide film, naturally formed when in air/aqueous solution, is attacked by chloride, most likely forming a porous film, maintaining zinc corrosion. It is well known[47-49] that chloride attacks the passive zinc oxide, forming pits, which would lead to a decrease in the open circuit potential values. However Abd El Aal[47] observed that the addition of small quantities of chloride to the solution does not alter the passive zinc oxide layer. In 0.010 mol L^{-1} NaCl solution at pH 5.5,[50] zinc dissolves forming Zn^{2+}, $ZnCl^{+}$ and $ZnOH^{+}$, rendering the surface practically oxide-free.

At pH 8-13 the zinc surface is covered by a passive ZnO layer, and from pH 6.3 to 7.7 the chloride salts would tend to form zinc hydroxychloride, and for pH > 7.7 ZnO is the most stable phase.[51] Therefore, ZnO is covering the electrode surface when the 0.1 mol L^{-1} NaCl solution at pH 11 was used.

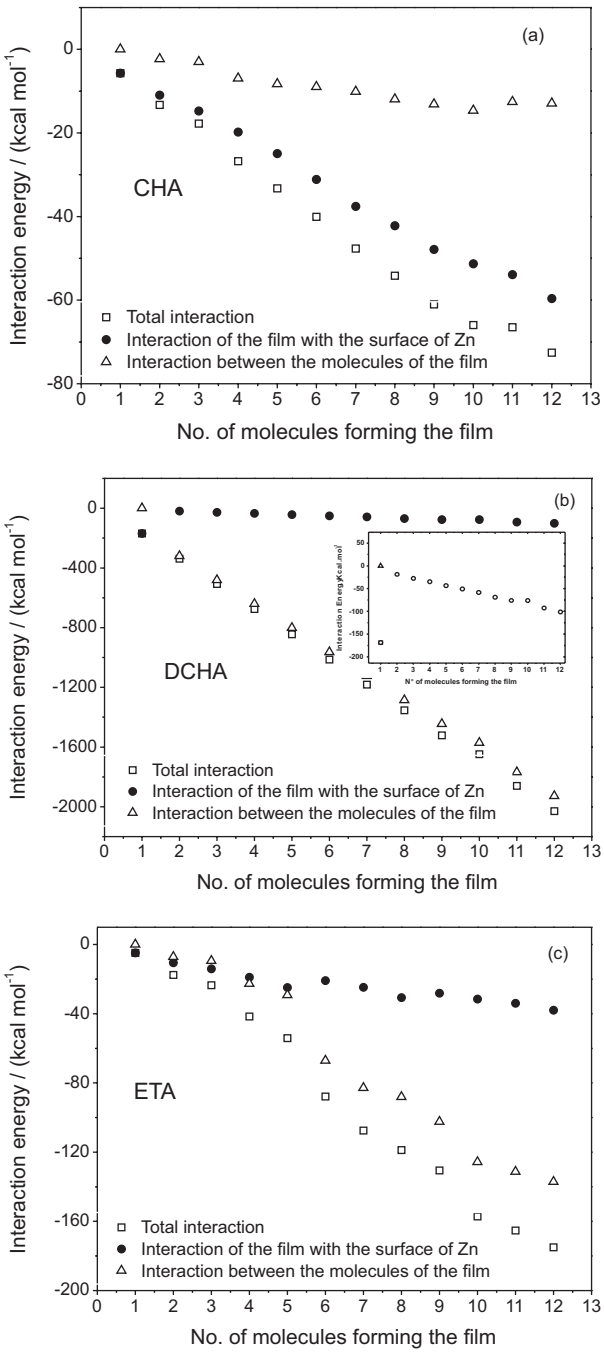

Figure 11. Interaction energy as a function of the number of VCI molecules, presented as: total interaction energy, energy between the molecules and the surface (vertical interaction) and energy between the molecules in the film (lateral interaction), for each VCI.

In order to investigate the presence of zinc oxides on the electrode surfaces, Raman spectra for zinc immersed in 0.1 mol L^{-1} NaCl solution at pH 6.5 and 11 in the presence and absence of inhibitors were recorded, and only the region from 200 to 1600 cm^{-1} is shown (Figure 14).

Raman analysis obtained for the zinc surface immersed in inhibitor-containing solution showed similar spectra with three main bands at around 331, 374, 437 and 1067 cm^{-1}.

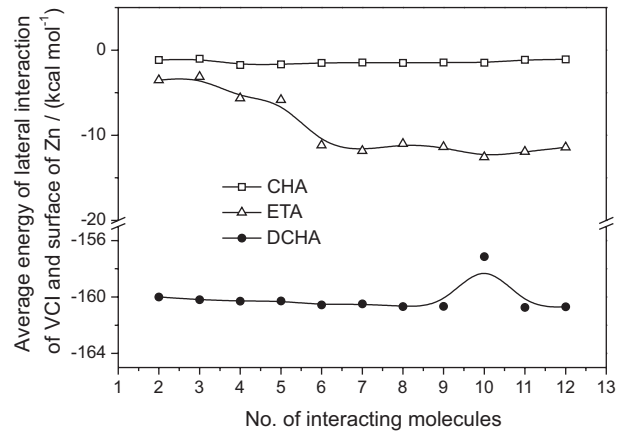

Figure 12. Average of the energy for the lateral interaction of VCIs on the zinc surface.

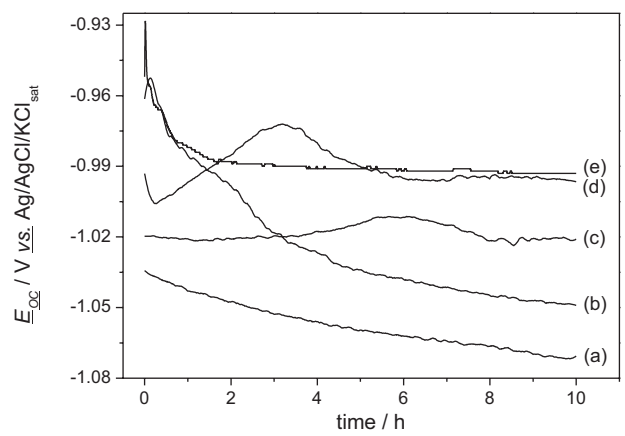

Figure 13. Open circuit potential for the zinc electrode in 0.1 mol L^{-1} NaCl pH 6.5 aqueous solution (a), pH 11 without the inhibitor (b) and with 5×10^{-3} mol L^{-1} VCI ETA (c); CHA (d) and DCHA (e).

The first three bands were attributed to ZnO[52,53] and the last one is probably related to the presence of a zinc hydroxychloride (simonkolleite, $Zn_5(OH)_8Cl_2$), constituting the main band of zinc hydroxychloride.[54] Raman analysis of the zinc electrode after immersion in NaCl solutions in the absence of inhibitors showed spectra dependent on the pH of the solution. The following bands were observed: 399, 438, 737, 1074, 1368, 1510 and 1552 cm^{-1} (pH 6.5) and 394, 437, 568, 846, 957, 1066, 1310, 1367, 1397 and 1512 cm^{-1} (pH 11), being the bands at 438 and 568 cm^{-1} characteristic of ZnO, and the bands at 1074 and 1066 cm^{-1} probably related to simonkelleite. The band at 568 cm^{-1} has been assigned to polycrystals of ZnO.[55,56] The bands at 399 and 737 cm^{-1} have been attributed to $Zn(OH)_2$.[57]

Electrochemical impedance spectroscopy (EIS)

Figure 15 shows EIS diagrams recorded for the zinc electrodes in 0.1 mol L^{-1} NaCl solution at pH 6.5 and 11 in the absence and presence of 5×10^{-5} mol L^{-1} VCIs.

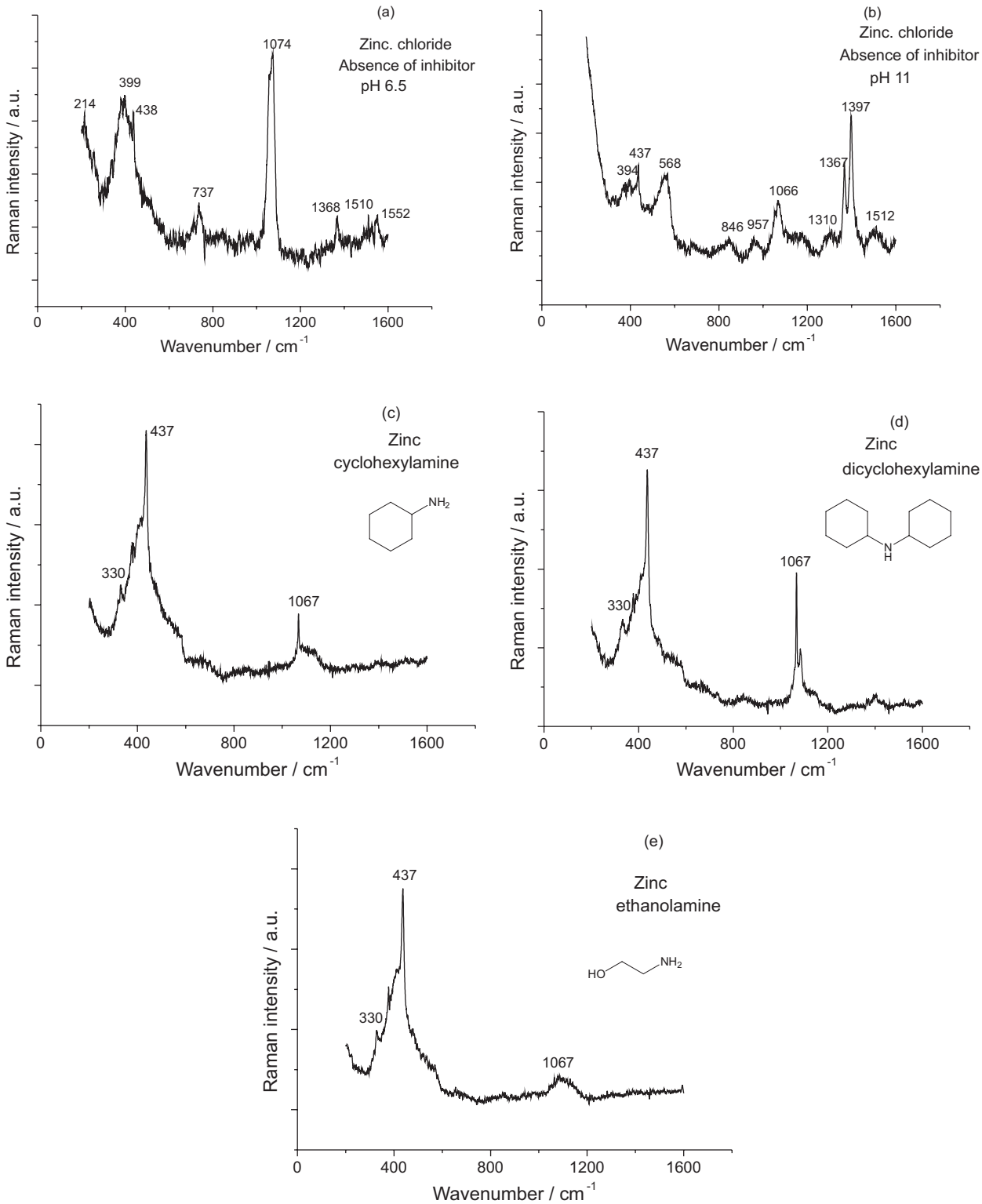

Figure 14. Raman spectra for the zinc surface after immersion in 0.1 mol L^{-1} NaCl solution at pH 6.5 (a), and at pH 11 in the absence (b) and presence of inhibitors: cyclohexylamine (c), dicyclohexylamine (d) and ethanolamine (e).

Figure 15a shows that the capacitive arcs obtained in the presence of the amines are greater than the ones from the NaCl solution (pH 11), indicating a polarization resistance increase promoted by these substances. In the Bode phase angle plots (Figure 15b) two time constants can be observed in the systems containing CHA, DCHA, ETA and NaCl (pH 11). Contrastingly, in NaCl (pH 6.5) solution, only one time constant is observed, at medium frequencies,

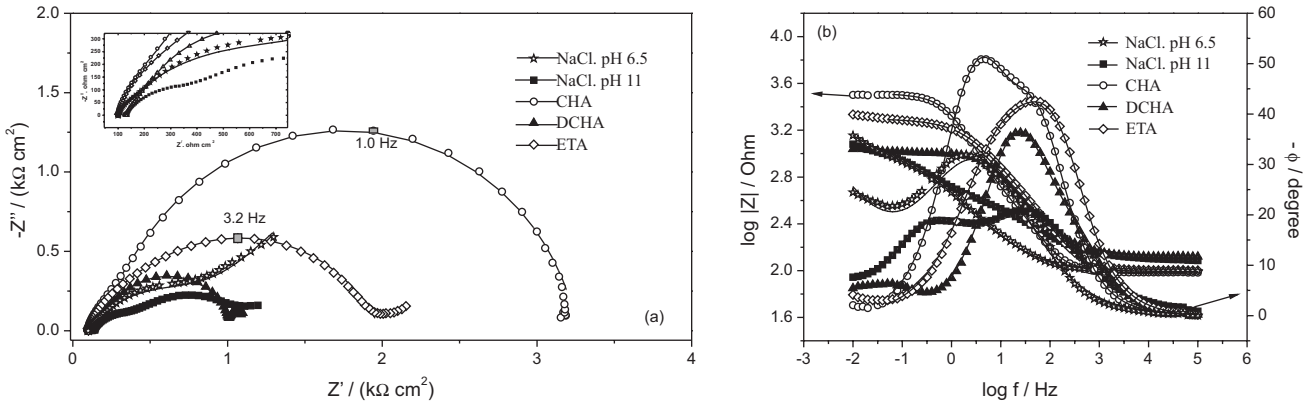

Figure 15. Experimental (symbol) and adjusted (solid line) complex plane diagrams (a) and Bode phase angle and modulus of impedance *vs.* log f plots (b) for the zinc electrodes in 0.1 mol L^{-1} NaCl solution at pH 6.5 and 11 in the absence and presence of 5×10^{-3} mol L^{-1} VCIs (CHA, DCHA and ETA).

followed by an increase in the modulus of impedance, |Z|, at low frequency, which indicates a diffusional contribution. In solution with pH 11, in the presence and absence of VCIs, Bode phase angle plots show two time constants and the Bode impedance modulus plot shows approximately constant values at low frequencies, indicating that diffusion process is not detected.

For a quantitative analysis of the impedance data, the equivalent electrical circuits (EEC) was employed, using the program developed by Boukamp.[35] In the choice of the EEC, the electrode/solution interfaces in this study are schematically represented in Figure 16. It is well known that active metals, such as zinc, aluminum, iron, etc., in contact with water or oxygen, spontaneously form an oxide layer over the surface (Figure 16b).

The thickness and properties of these oxides depend on the metal and under which physical conditions they are submitted (temperature, exposure time) and the composition of the environment surrounding the metal.[21] As already described, Raman data confirm the presence of zinc oxide, and possibly simonkolleite on the zinc surface, especially at pH 11 and in the presence of the VCIs, while it is less likely that this oxide or chlorohydroxide layer is formed at a high quantity when the electrode is immersed

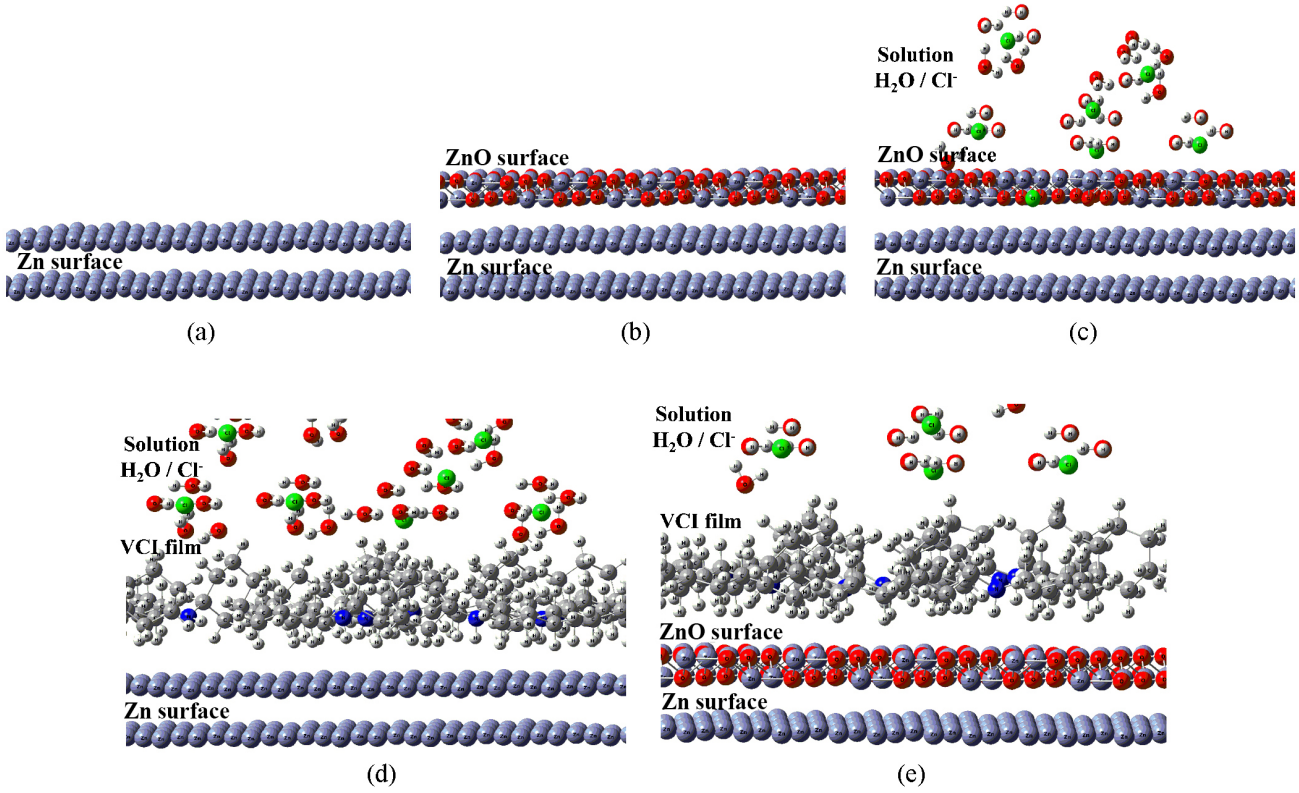

Figure 16. Representative scheme of the zinc surface (a) suffering interaction with: the zinc oxide layer (b); zinc oxide layer + water + chloride (c); VCI protective film + water + chloride (d); zinc oxide layer + VCI protective film + water + chloride (e).

in a pH 6.5 solution, as previously described. Thus, if this oxide exists at pH 6.5, it is likely to be a porous oxide, and at pH 11, this oxide exhibits the properties of a passive film in low chloride concentration solutions (Figure 16c).

For the pH 11 solution, the zinc oxide layer is thicker on the zinc surface and with a smaller concentration of defects, which slows down the chloride permeation through the layer and thus, reduces chloride attack on zinc. In the presence of the amines on vapor form, there should be the formation of a VCI layer at the zinc/zinc oxide surface, due to condensation of these compounds (Figure 16d, e). In the systems where CHA and ETA are present, there could also be water vapor condensation. Therefore, it is possible that hydroxyl ions are formed, as described by equations 1 and 2.[20,58] The excess of OH^- groups interacts with Zn^{2+} to form zinc hydroxides, which consequently can form several zinc oxide/zinc hydroxide as proposed by the reactions in the equations 11-13.[58]

$$Zn^{2+} + 2\ OH^- \leftrightarrow Zn(OH)^2 \quad (11)$$

$$Zn(OH)_2 \leftrightarrow ZnO\downarrow + H_2O \quad (12)$$

$$ZnO + H_2O + 2OH^- \leftrightarrow [Zn(OH)_4]^{2-} \quad (13)$$

Besides the $Zn(OH)_2$ and $[Zn(OH)_4]^{2-}$species, $[Zn(OH)_2]^-$ can also be formed.[20] This could be attributed to the strong basicity of these compounds and also the Zn^{2+} complexation. Zinc hydroxide formation (equation 11) causes the protonation of CHA (equation 2) and consequently more hydroxide ions are made available for the environment.

DCHA presents extremely low solubility,[32] and therefore, its protonation and hydroxide release could be considered inferior to CHA and ETA. This could explain the greater protective effect of DCHA, for it has an equilibrium displacement of equation 3 to its right side when compared with CHA (equation 2) and ETA (equation 1),[20,32,58] and this could decrease the formation of zinc hydroxides.

The impedance experimental data were analyzed using the EEC shown in Figure 17 and the parameter values of the EEC are shown in Table 4. The low values of χ^2, around 10^{-4}, indicate that a good fitting was obtained between the experimental data and the present model as shown in Figure 15.

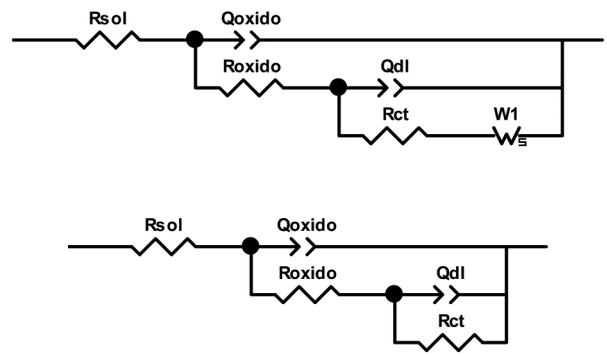

Figure 17. EECs used to adjust the EIS diagrams of Figure 15: (a) for NaCl solution at pH 6.5 and (b) for NaCl solution at pH 11 in the absence and presence of VCI (CHA, DCHA and ETA).

The parameters related to the zinc oxide/hydroxide are almost independent of the experimental condition used with an exponent value around 0.8, indicating a heterogeneous electrical property distribution through the oxide layer with an admittance around 10^{-4} S cm^{-2} s^n, and oxide resistance from 200 to 600 Ω cm^2. The admittance related to the capacitance of the electrical double layer was found to be around 10^{-5} S cm^{-2} s^n for the zinc electrode in the presence of VCIs and higher values were found in their absence. The charge transfer resistance is higher in the presence of VCIs, suggesting that the zinc dissolution is delayed by the adsorption of VCI on the ZnO, as already suggested by the theoretical studies.

Scanning electron microscopy

Figure 18 shows secondary electron micrographs obtained with 5000× magnification for the zinc surface after 15 days of immersion in 0.1 mol L^{-1} NaCl aqueous solution, in the presence and absence of the VCIs. Different deposits are clearly observed over the surface, depending on the VCI. Despite the visual difference, chemical analysis shows the presence of zinc and oxygen in these deposits, and the

Table 4. EEC parameters and variance of the residual error obtained for zinc electrodes in 0.1 mol L^{-1} NaCl solution in the presence and absence of 5×10^{-3} mol L^{-1} VCI

Solution	Q_{oxide}			Q_{dl}					
	R_{sol} / (Ω cm^2)	Y_2 / (S cm^{-2} s^n)	n_2	R_{oxid} / (kΩ cm^2)	Y_3 / (S cm^{-2} s^n)	n_3	R_{CT} / (kΩ cm^2)	W / (Ω cm^2 s$^{0.5}$)	$\div^2$
NaCl, pH 6.5	99	1.9×10^{-4}	0.79	0.2	4.5×10^{-4}	0.74	0.5	4.7×10^{-3}	2.2×10^{-4}
NaCl, pH 11	122	2.0×10^{-4}	0.80	0.4	1.0×10^{-3}	0.70	0.6	–	2.0×10^{-4}
NaCl, ETA, pH 11	100	1.7×10^{-4}	0.87	0.5	7.5×10^{-5}	0.69	1.4	–	2.1×10^{-5}
NaCl, CHA, pH 11	96.1	3.1×10^{-5}	0.89	0.6	4.5×10^{-5}	0.90	2.5	–	8.5×10^{-5}
NaCl, DCHA, pH 11	131	2.2×10^{-5}	0.84	0.2	2.7×10^{-5}	0.84	0.7	–	4.7×10^{-5}

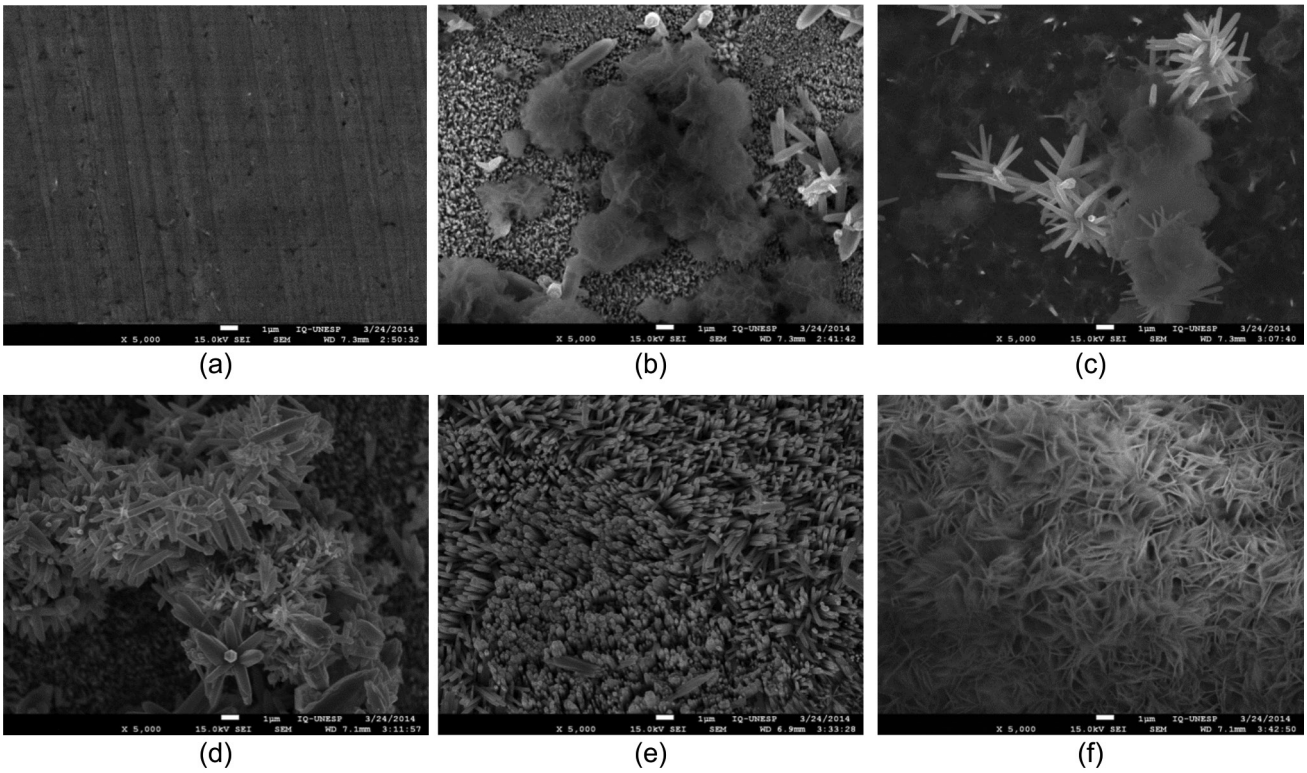

Figure 18. Zinc surface micrographs after 15 days of immersion in 0.1 mol L^{-1} NaCl solution in the presence and absence of the inhibitors at 5×10^{-3} mol L^{-1} concentration. (a) Post polishing; (b) NaCl, pH 6.5; (c) NaCl, pH 11; (d) NaCl + CHA; (e) NaCl + DCHA; and (f) NaCl + ETA. Magnification: 5000×.

samples immersed in NaCl only (Figure 18b, c) showed the presence of chloride on the surface. The presence of these elements on the surface suggest the formation of zinc oxides, zinc hydroxides and the simonkolleite corrosion product.[54,59] Carbon atoms were not detected, which could be associated with the volatility of the VCIs. Chloride was not detected in the presence of the VCIs, suggesting some degree of protection to the zinc/zinc oxide surface.

Accelerated corrosion assay - wet chamber

After sample conditioning during 7 days in the wet chamber, 80× magnification images were obtained (Figure 19). Generally, the zinc samples suffered some kind of attack, which was or was not minimized by the VCI action. It can be noted that DCHA (Figure 19d) shows greater protective effect at zinc surface against corrosion, for it shows some similarity to the sample surface before the assay (Figure 19a). On the other hand, it is observed that zinc in the presence of ETA vapor (Figure 19e) shows generalized corrosion. CHA-treated zinc (Figure 19c) displays corrosion for almost the entire surface, but non-attacked and mildly attacked regions could be identified. Therefore, it is possible to infer from the images the following order for VCI corrosion inhibition efficiency: DCHA > CHA >> ETA.

The action of the vapors happens by the condensation of the VCI.[39] For this situation, the solubility of the compounds, so crucial in the EIS assays, is not relevant. This results in a much greater protective effect from DCHA, which greatly differs from the EIS results (Table 4), but agrees with the theoretical results, with respect to the frontier molecular orbitals (smaller HOMO-LUMO gap) and also by the strong interaction energy. For CHA and ETA, it could be verified that their vapors could not avoid the destructive action of chloride over the zinc/zinc oxide surface, but despite this fact, the inhibition efficiency could be considered satisfactory, under the EIS assays view, which can be attributed to the action of the amine groups, along with the pH raise, suggesting that accelerated corrosion assays in the wet chamber show the same tendency observed in the computational simulations.

Conclusions

The synergistic use of DFT level quantum mechanical calculations, electrochemical assays, scanning electron microscopy and wet chamber assays allowed us to evaluate the VCI compounds CHA, DCHA, ETA about the protective/destructive interaction at the zinc/zinc oxide surface.

Theoretical calculations of the VCI in contact with the zinc surface demonstrate that DCHA interacts strongly with

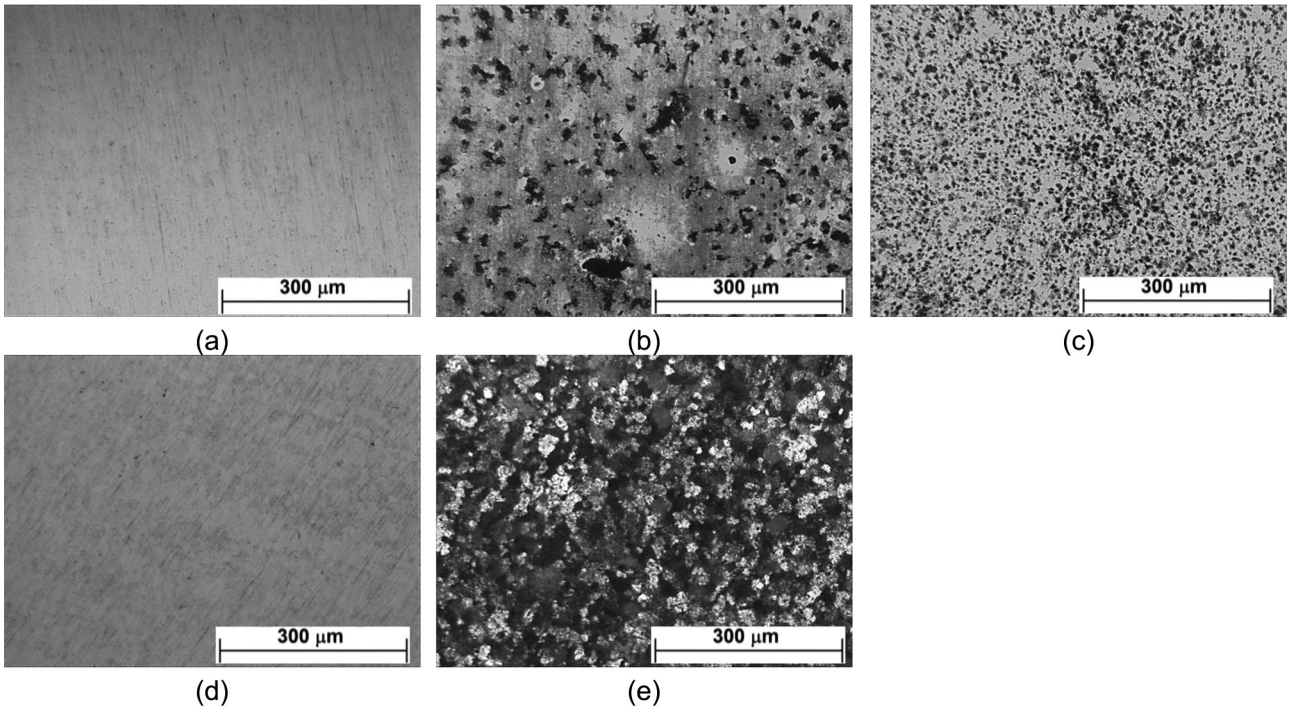

Figure 19. Zinc surface micrographs after wet chamber conditioning for 7 days, in the presence and absence of the VCIs: (a) after polishing; (b) without inhibitor; (c) CHA; (d) DCHA; and (e) ETA at 80× magnification.

the zinc surface, differently from ETA, where the interaction was much inferior. Furthermore, the six-membered ring shape organization for CHA and ETA and five and six-membered ring shapes organization for DCHA were observed.

The solubility of the compounds must be taken into account when studying the phenomenon in solution. Therefore, DCHA does not offer a good protective effect, for its solubility is extremely low. In contrast, CHA shows a greater solubility in water, and thus, shows greater resistance to charge transfer. ETA in solution presented inferior charge transfer resistance compared to CHA. These compounds raise the pH of the solution, which is another determinant factor for the observed protective effect.

Wet chamber assays allowed verifying that DCHA protected zinc from corrosion, while CHA and ETA did not, allowing the partial or total corrosion of the zinc sample, especially ETA where generalized corrosion could be found.

The protective action of the inhibitors is linked to the environment into which the sample is inserted. Therefore, the most efficient VCI is DCHA, which agrees with the theoretical predictions.

Acknowledgments

We gratefully acknowledge the Brazilian research agency CAPES for financial support, LMA-IQ UNESP for FEG-SEM facilities and GRID-UNESP, and CNPq (proc. No. 305890/2010-7) for scholarship.

References

1. Subramanian, A.; Rajendran, P.; Natesan, N.; Balakrishnan, K.; Vasudevan, T.; *Anti-Corros. Methods Mater.* **1999**, *46*, 346.
2. Rammelt, U.; Koehler, S.; Reinhard, G.; *Corros. Sci.* **2009**, *51*, 921.
3. Gómes, B.; Likhanova, N. V.; Dominguez, A. M. A.; Olivares, O.; Hallen, J. M.; Martinez, M. J. M.; *J. Phys. Chem.* **2005**, *109*, 8950.
4. Quraishi, M. A.; Sardar, R.; Rawat, J.; *Mater. Chem. Phys.* **2002**, *79*, 603.
5. Vuorinen, E.; Kálmán, E.; Focke, W.; *Surf. Eng.* **2004**, *20*, 280.
6. Bastidas, D. M.; Cano, E.; Mora, E. M.; *Anti-Corros. Methods Mater.* **2005**, *52*, 71.
7. Hallik, A.; Alumaa, A.; Tamm, J.; Sammelselg, V.; Väärtnõu, M.; Jänes, A.; Lust, E.; *Synth. Met.* **2006**, *156*, 488.
8. Dąbrowski, A.; *Adv. Colloid Interface Sci.* **2001**, *93*, 135.
9. Jafari, H.; Danaee, I.; Eskandari, H.; Rashvand, A. M.; *Ind. Eng. Chem. Res.* **2013**, *52*, 6617.
10. International Electrotechnical Comission (IEC); *IEC 60068-2-30: Basic Environmental Testing Procedures, Part 2: Tests - Test Db and Guidance: Damp Heat, Cyclic (12 + 12-Hour Cycle)*; IEC: Geneva, 1980.
11. Peres, N.; *Electrochemistry and Corrosion Science*; Kluwer Academic Publishers: Boston, 2004.
12. Bürger, A.; Magdans, U.; Gies, H.; *J. Mol. Model.* **2013**, *19*, 851.
13. Gece, G.; *Corros. Sci.* **2008**, *50*, 2981.
14. Emreguel, K. C.; Abduelkadir, A. A.; Atakol, O.; *Mater. Chem. Phys.* **2005**, *93*, 325.

15. Dapprich, S.; Komáromi, I.; Byun, K. S.; Morokuma, K.; Frisch, M. J.; *J. Mol. Struct.* **1999**, *461*, 1.
16. Rassolov, V. A.; Pople, J. A.; Ratner, M. A.; Windus, T. L.; *J. Chem. Phys.* **1988**, *109*, 1223.
17. Mitnik, D. G.; Lucero, A. M.; *J. Mol. Struct.* **2001**, *536*, 41.
18. Tang, H.; Fan, K.; *Chem. Phys. Lett.* **2000**, *330*, 509.
19. Matczak, P.; *Comput. Theor. Chem.* **2013**, *1013*, 7.
20. Bagabas, A.; Alshammari, A.; Aboud, M. F. A.; Kosslick, H.; *Nanoscale Res. Lett.* **2013**, *8*, 516.
21. Lukovits, I.; Kalman, E; Zucchi, F.; *Corrosion* **2001**, *57*, 3; Wöll, C.; *Prog. Surf. Sci.* **2007**, *82*, 55.
22. Gao, Y.; Zhao, N.; Wei, W.; Sun, Y.; *Comput. Theor. Chem.* **2012**, *992*, 1.
23. Vo, C. T.; Huynh, L. K.; Hung, J.; Jiang, J.; *Appl. Surf. Sci.* **2013**, *280*, 219.
24. Lewars, E.; *Computational Chemistry: Introduction to the Theory and Applications of Molecular and Quantum Mechanics*; Kluwer Academic Publishers: New York, 2003.
25. Frisch, M. J.; Trucks, G. W.; Schlegel, H. B.; Scuseria, G. E.; Robb, M. A.; Cheeseman, J. R.; Scalmani, G.; Barone, V.; Mennucci, B.; Petersson, G. A.; Nakatsuji, H.; Caricato, M.; Li, X.; Hratchian, H. P.; Izmaylov, A. F.; Bloino, J.; Zheng, G.; Sonnenberg, J. L.; Hada, M.; Ehara, M.; Toyota, K.; Fukuda, R.; Hasegawa, J.; Ishida, M.; Nakajima, T.; Honda, Y.; Kitao, O.; Nakai, H.; Vreven, T.; Montgomery, J. A., Jr.; Peralta, J. E.; Ogliaro, F.; Bearpark, M.; Heyd, J. J.; Brothers, E.; Kudin, K. N.; Staroverov, V. N.; Kobayashi, R.; Normand, J.; Raghavachari, K.; Rendell, A.; Burant, J. C.; Iyengar, S. S.; Tomasi, J.; Cossi, M.; Rega, N.; Millam, M. J.; Klene, M.; Knox, J. E.; Cross, J. B.; Bakken, V.; Adamo, C.; Jaramillo, J.; Gomperts, R.; Stratmann, R. E.; Yazyev, O.; Austin, A. J.; Cammi, R.; Pomelli, C.; Ochterski, J. W.; Martin, R. L.; Morokuma, K.; Zakrzewski, V. G.; Voth, G. A.; Salvador, P.; Dannenberg, J. J.; Dapprich, S.; Daniels, A. D.; Farkas, Ö.; Foresman, J. B.; Ortiz, J. V.; Cioslowski, J.; Fox, D. J.; *Gaussian 09, Revision D.01*; Gaussian, Inc., Wallingford CT, 2009.
26. Becke, A. D.; *Phys. Rev. A: At., Mol., Opt. Phys.* **1988**, *38*, 3098.
27. Rassolov, V. A.; Ratner, M. A.; Pople, J. A.; Redfern, P. C.; Curtiss, L. A.; *J. Comput. Chem.* **2001**, *22*, 976.
28. Dennington, R.; Keith, T.; Milliam, J.; *GaussView, Version 5*; Semichem Inc., Shawnee Mission KS, 2009.
29. Cossi, M.; Rega, N.; Scalmani, G.; Barone, V.; *J. Comput. Chem.* **2003**, *24*, 669.
30. Tomasi, J.; Mennucci, B.; Cammi, R.; *Chem. Rev.* **2005**, *105*, 2999.
31. Macedo, M. C. S. S.; Barcia, O. E.; Da Silva, E. C.; Mendes, J. O.; Mattos, O. R.; *J. Electrochem. Soc.* **2012**, *159*, C160.
32. Rosenfeld, I. L.; Persiantseva, V. P.; *Ingibitory Atmosfernoi Korrozii*; Nauka: Moscow, 1985.
33. Ibatullin, K. A.; Andreev, N. N.; *Prot. Met.* **2002**, *38*, 13.
34. Cachet, C.; Ganne, F.; Maurin, G.; Petitjean, J.; Vivier, V.; Wiart, R.; *Electrochim. Acta* **2001**, *47*, 509.
35. Boukamp, B. A.; *Equivalent Circuit Users Manual*; University of Twente: Enschede, 1989.
36. Ormellese, M.; Lazzari, L.; Goidanich, S.; Fumagalli, G.; Brenna, A.; *Corros. Sci.* **2009**, *51*, 2959.
37. Ebenso, E. E.; Arslan, T.; Kandemirli, F.; Love, I.; Öğretir, C.; Saracoğlu, M.; Umoren, S. A.; *Int. J. Quantum Chem.* **2010**, *110*, 2614.
38. Mohammad, B. G.; Maryam, T.; Ghodratollah, M.; *Anal. Chim. Acta* **2012**, *713*, 36.
39. Koopmans, C. T.; *Physica* **1934**, *1*, 104.
40. Pearson, R. G.; *Inorg. Chem.* **1988**, *27*, 734.
41. Larabi, L.; Benali, O.; Mekelleche, S. M.; Harek, Y.; *Appl. Surf. Sci.* **2006**, *253*, 1371.
42. Field, M. J.; Bash, P. A.; Karplus, M.; *J. Comput. Chem.* **1990**, *11*, 700.
43. Mulliken, R. S.; *J. Chem. Phys.* **1955**, *23*, 1833.
44. Hratchian, H. P.; Parandekar, P. V.; Raghavachari, K.; Frisch, M.; Vreven, T.; *J. Chem. Phys.* **2008**, *128*, 34107.
45. Zheludkevich, M. L.; Yasakau, K. A.; Poznyak, S. K.; Ferreira, M. G. S.; *Corros. Sci.* **2005**, *47*, 3368.
46. Boulet, P.; Knöfel, C.; Kuchta, B.; Hornebecq, V.; Llewellyn, P. L.; *J. Mol. Model.* **2012**, *18*, 4819.
47. Abd El Aal, E. E.; *Corros. Sci*. **2000**, *42*, 1.
48. Peulon, S.; Lincot, D.; *J. Electrochem. Soc.* **1998**, *145*, 864.
49. Abd El Aal, E. E.; *Corros. Sci*. **2004**, *46*, 37.
50. Tada, E.; Sugawara, K.; Kaneko, H.; *Electrochim. Acta* **2004**, *49*, 1019.
51. Thomas, S.; Birbilis, N.; Venkatraman, M. S.; Cole, I. S.; *Corrosion* **2012**, *68*, 015009-1.
52. Gandikota, V.; Xing, Y.; *Adv. Nanopart.* **2014**, *3*, 5.
53. Devaraj, R.; Karthikeyan, K.; Jeyasubramanian, K.; *Appl. Nanosci.* **2013**, *3*, 37.
54. Autengruber, R.; Luckeneder, G.; Hassel, A. W.; *Corros. Sci.* **2012**, *63*, 12.
55. Cusco, R.; Alarcon-Llado, E.; Ibanez, J.; Artus, L.; Jimenez, J.; Wang, B.; Callahan, M. J.; *Phys. Rev. B: Condens. Matter Mater. Phys.* **2007**, *75*, 165202.
56. Bernard, M. C.; Hugot-Le Goff, A.; Phillips, N.; *J. Electrochem. Soc.* **1995**, *142*, 2162.
57. Bernard, M. C.; Hugot-Le Goff, A.; Phillips, N.; *J. Electrochem. Soc.* **1995**, *142*, 2167.
58. Wang, X.; Zhang, Q.; Wan, Q.; Dai G.; Zhou, C.; Zou, B.; *J. Phys. Chem. C.* **2011**, *115*, 2769.
59. El-Turki, A.; Allen, G. C.; Hallam, K. R.; *Br. Corros. J.* **2001**, *36*, 191.

Submitted: July 17, 2014
Published online: December 19, 2014

FAPESP has sponsored the publication of this article.